Available online at www.sciencedirect.com

SciVerse ScienceDirect

Physics Procedia 37 (2012) 1349 – 1354

Physics Procedia

TIPP 2011 – Technology and Instrumentation in Particle Physics 2011

An Absorber-coupled TES Bolometer for Measuring CMB Polarization

G. Wang[a*], V. Yefremenko[b], V. Novosad[b], J. Pearson[b], R. Divan[c], C. L. Chang[a,d], L. Bleem[d], A. T. Crites[d], J. Mehl[d], B. A. Benson[d], T. Natoli[d], K. Story[d], S. S. Meyer[d], J. E. Carlstrom[a,d], J. McMahon[e], J. Sayre[f], J. Ruhl[f], E. George[g], N. Harrington[g], C. Reichardt[g], E. Shirokoff[g], E. Young[g], A. Lee[g], and W. Holzapfel[g]

[a]*High Energy Physics Division, Argonne National Laboratory, 9700 S Cass Ave., Argonne, IL 60439, USA*
[b]*Materials Science Division, Argonne National Laboratory, 9700 S Cass Ave., Argonne, IL 60439, USA*
[c]*Center for Nanoscale Materials, Argonne National Laboratory, 9700 S Cass Ave., Argonne, IL 60439, USA*
[d]*Kavli Institute for Cosmological Physics, the University of Chicago, 5640 S Ellis Ave., Chicago, IL 60637, USA*
[e]*Department of Physics, University of Michigan, 450 Church St., Ann Arbor, MI 48109, USA*
[f]*Department of Physics, Case Western Reserve University, 10900 Euclid Ave., Cleveland, OH 44106, USA*
[g]*Department of Physics, University of California, LeConte Hall, Berkeley, CA 94720, USA*

Abstract

We report an absorber-coupled superconducting Transition Edge Sensor (TES) bolometric polarimeter for measuring Cosmic Microwave Background (CMB) B-mode polarization. The polarimeter consists of a dipole-like PdAu absorber and a Mo/Au bi-layer TES on a suspended silicon nitride rectangle. Its design, fabrication, thermal properties, and optical performance are presented.

Keywords: Bolometer; Transition edge sensor; Heat transport; CMB.

1. Introduction

Superconducting TES bolometers can used to measure thermal fluctuations on the sky through a variety of radiation coupling mechanisms [1]. A TES operated with negative electro-thermal feedback

* E-mail: gwang@anl.gov

1875-3892 © 2012 Published by Elsevier B.V. Selection and/or peer review under responsibility of the organizing committee for TIPP 11.
Open access under CC BY-NC-ND license. doi:10.1016/j.phpro.2012.02.468

under a voltage bias can be tuned to have a fast response time and a noise level below the photon shot noise [1-3]. Therefore a TES bolometer, with appropriate optical coupling, has the performance required to conduct sensitive observation of the cosmic microwave background radiation.

We have developed an absorber-coupled TES bolometric polarimeter with a 30% optical bandwidth at 90 GHz. An array of 180 of these polarimeters will be deployed on the South Pole Telescope (SPT) as part of a new polarization camera for the SPTpol experiment. The two key scientific goals of SPTpol are to detect the CMB B-mode polarization induced by inflationary gravitational waves, which would provide a direct measurement of the energy scale of inflation [4-5], and to measure the sum of neutrino masses through gravitational lensing of the CMB by large-scale structures in the universe [6].

2. Detector Design and Fabrication

The absorber-coupled polarimeter is designed for 90 GHz and consists of a dipole-like photon absorber for optical coupling and a Mo/Au bi-layer superconducting TES for thermal energy readout on a 1 μm thick Si_3N_4 rectangle. Four 10 μm wide and 640 μm long Si_3N_4 legs at the TES sensor side and two 10 μm wide and 640 μm long Si_3N_4 legs at the opposite side support the rectangle and serve as the weak thermal link to the cryogenic heat bath. The thermal conductance is G=170 pW/K at 530 mK, which has a phonon noise comparable to the photon noise for ground-based observations. Fig. 1 (a) is a single-polarization detector. The dual-polarization pixel is a face-to-face setup of two single-polarization detectors perpendicular to each other and with a separation of 40 μm.

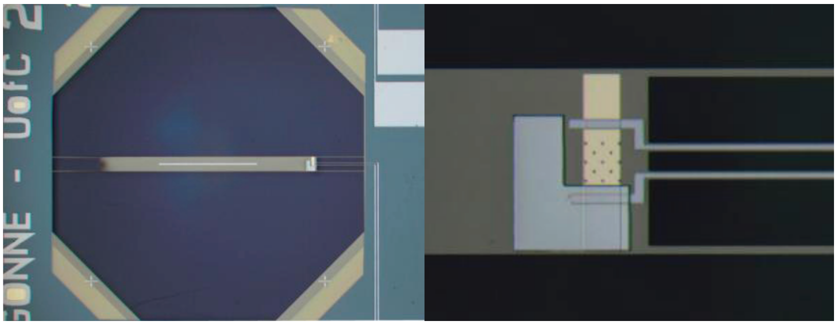

(a) (b)

Fig. 1. (a) A 90 GHz absorber-coupled TES polarimeter. A 1320 μm by 18 μm dipole-like PdAu absorber is in the middle of the 2940 μm by 200 μm Si_3N_4 rectangle with six support legs. A TES is at the right end of the rectangle; (b) A magnified picture of the TES, which is 70 μm by 40 μm between the leads. The Nb dots on the top are for modifying TES superconducting transition width. For stable operation an additional thermal mass of 400 nm thick PdAu bling is connected to the TES at the lower side.

For the polarimeter, the beam is defined by a feed horn and telescope optics, which couples radiation from the sky into a circular waveguide. The band-pass is defined at the low end by the waveguide cut-off and at the high end by a free space metal mesh filter placed in front of the horn. The radiation in the waveguide is coupled to the TES through the absorber located on a Si_3N_4 membrane which spans the guide λ/4 from a backshort. A waveguide choke prevents the fields from leaking out of the guide where the membrane penetrates. This design was optimized using High Frequency Structure Simulator (HFSS) to have a larger than 95% co-polar coupling and a less than 1% cross-polar coupling across the entire band. The present design uses a 78 GHz waveguide cut-off and a 110 GHz metal mesh low pass filter.

The detector fabrication is performed at the Materials Science Division and at the Center for Nanoscale Materials, Argonne National Laboratory. We purchase commercial 250 μm thick silicon wafers with 1 μm thick low stress silicon nitride on both sides from Rogue Valley Microelectronics. First we fabricate the Mo/Au bi-layer superconducting TES sensor with DC magnetron sputtering and standard photolithography techniques. The Mo is 22 nm thick, and Au 30 nm thick. The Nb dots on top of the TES and the 5 μm wide and 120 nm thick Nb leads are patterned with lift-off. Next the PdAu absorber is fabricated with DC magnetron sputtering and lift-off. The thickness of PdAu is chosen to give a sheet impedance of 5.3 Ω/□ at operational cryogenic temperature. HFSS simulation shows that this impedance optimizes optical absorption of the polarimeter. The silicon behind the rectangle and the support legs is removed by KOH etching. The Si_3N_4 legs are patterned with Reactive Ion Etch (RIE).

2. Detector Thermal Properties

The bolometric detector thermal conductance is defined by Si_3N_4 support beams dimension and thermal conductivity. For a given Si_3N_4 beam, its thermal conductance is

$$G = \kappa A/L, \tag{1}$$

where L is the beam length, A is cross section, κ is thermal conductivity. In the phonon gas kinetic theory,

$$\kappa = ClS/3, \tag{2}$$

where C is Si_3N_4 volume heat capacity, l is phonon mean free path, and $S=6986\ m/s$ is the average Si_3N_4 sound speed calculated with its longitudinal and transverse sound speeds [7].

Si_3N_4 thermal conductivity is investigated using tailored thermal structures with TES on an island [8]. Empirically, the heat power flow along the beam as a function of bath temperature for a defined thermal structure is fitted as a power law [9-12] of

$$P = K(T^n - T_b^{\ n}), \tag{3}$$

where coefficient K and temperature power index n characterize thermal conductance, T is the temperature at the sensor, T_b is the bath temperature. In our investigation temperature range, we assume a power law dependence of thermal conductivity on temperature. The thermal conductance is the first derivative of the power over temperature,

$$G = nKT^{n-1}. \tag{4}$$

Therefore, thermal conductivity is connected with experimental data using equations (1) and (4) as

$$\kappa = (L/A)nKT^{n-1}. \tag{5}$$

For the polarimeter in Fig.1 (a), assuming that heat conduction obeys equation (3) for a single support beam and the PdAu absorber is isothermal, TES Joule heating power as a function of bath temperature is

$$P = 4K(T^n - T_b^{\ n}) + G_1 \frac{G_2 2K(T^n - T_b^{\ n}) - P_0(G_2 + 2nKT^{n-1})}{(G_1 + G_2)(G_2 + 2nKT^{n-1}) - G_2^{\ 2}}, \tag{6}$$

where T is TES temperature, $P_0=0$ is optical power in dark test, G_1 is the thermal conductance from the TES to the absorber, G_2 is the thermal conductance from the absorber to the end of the rectangle on the left. The values of G_1 and G_2 are estimated using TES temperature, the polarimeter dimensions and model data from reference [8] to the first order.

We have made and tested tailored thermal structures with 10 μm to 30 μm beam width, and five types of polarimeters. Four of the polarimeters have Si_3N_4 beams widths of 10 μm, 12 μm, 15 μm and 20 μm. The fifth polarimeter has two different beam width: two 30 μm beams and two 15 μm beams at the TES side, and two 30 μm beams at the far side [13]. TES transition temperature varies from 460 mK to 550 mK, and we vary the cryogenic bath temperature from 300 mK to close to TES transition temperature. The thermal conductivities for a variety of beams at 450 mK are shown in Fig. 2 (a). There are three classes of data. The crosses are the thermal tested structures [8] and the circles are the polarimeters [13] with Si_3N_4 grown on B1562, a common commercial 250 μm Si wafer. Finally the squares are the polarimeters with Si_3N_4 grown on B3663 which is high quality 250±5 μm Si wafer.

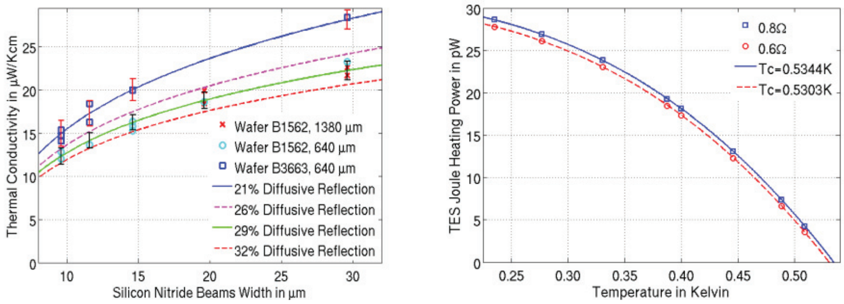

Fig. 2. Beam width dependence of thermal conductivity of 1 μm Si_3N_4 at 0.450 K. The beam width is shifted down 0.4 μm from nominal values because of side etching effects; (b) TES Joule heating power as a function of bath temperature using equation (6) at TES resistance of 0.8 Ω (K=34.15 pW/K^n, n=2.98) and 0.6 Ω (K=34.05 pW/K^n, n=2.98) respectively for a polarimeter in Fig. 1.

The boundary limited phonon transport model [14] is used to interpret the data. The green central line for the data of wafer B1562 is the model at 29% surface diffusive reflection of phonons. The two dashed lines show that the thermal conductivity is in ±3% surface diffusive reflection range. The phonon mean free path is estimated to be 6.58 μm, 9.80 μm and 11.55 μm for beams with width of 10 μm, 20 μm and 30 μm respectively for wafer B1562. In the theory of boundary limited phonon transport model, we may assume a beam width independent heat capacity. The Si_3N_4 volume heat capacity is estimated to be $0.082T+0.502T^3$ J/m^3-K [13]. The thermal conductivity for wafer B3663 has similar beam width dependence at 21% surface diffusive reflection.

In our detector fabrication for deployment on SPTpol, we have been using Si_3N_4 with thermal conductivity similar to that of wafer B1562. Fig. 2 (b) shows the TES Joule heating power as a function of bath temperature of one polarimeter using equation (6). The TES has a R – T relation in Fig. 3 (b). At T=0.450 K, the 10 μm beam thermal conductivity is 12.87 μW/Kcm using the fit at R=0.6 Ω.

2. Detector Performance

One focus of the polarimeter development has been on controlling the TES transition width. For stable operation the width must be broader than that provided by the Mo/Au TES alone. Fig. 3 (a) shows TES transition width dependence on modification structures. All TESs have two-side PdAu bling. The blue circles are measued using 4-wire method, the others using SQUIDs. The blue circles are for a TES without surface modification. The green squares are for a TES with a 3 μm wide Nb bar in the middle. The magenta diamonds are for a TES with three 3 μm wide Nb bars and 18 μm spacing. The red triangles are for a TES with 3 μm diameter Nb dots and 11 μm row spacing. We find that the three Nb bars with 18 μm spacing slightly increases TES transition width and the 3 μm diameter Nb dots with 11 μm row spacing significantly increases TES transition width. The lateral proximity effect [15] and the tunneling superconducting current between Nb structures [16] may have roles in the TES transition width.

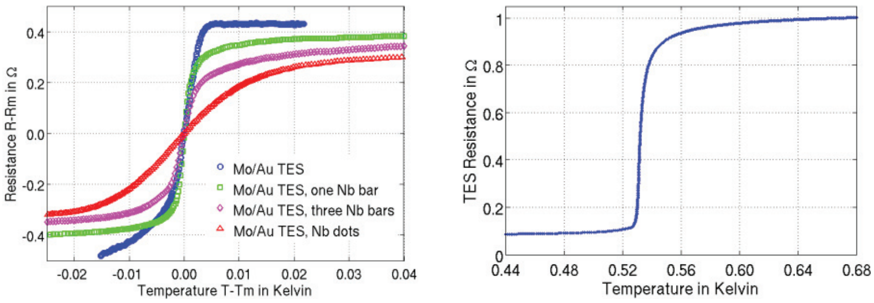

(a) (b)

Fig. 3. (a) 23nm Mo and 30nm Au bi-layer TES transition width dependence on surface modification structures. Rm=0.645 Ω and Tm=0.541 K for blue circles, Rm=0.552 Ω and Tm= 0.554 K for green squares, Rm= 0.495 Ω and Tm= 0.556 K for magenta diamonds, Rm= 0.450 Ω and Tm=0.565 K for red triangles; (b) 22nm Mo and 30nm Au bi-layer TES resistance – temperature relation, the TES has one side PdAu bling and Nb dots with 18 μm row spacing as shown in Fig. 1 (b).

Based on these results, we successfully use 3 μm diameter Nb dots with 18 μm row spacing on top of the TES to define the transition width. Fig. 3 (b) shows the R-T relation of a TES. The 90 mΩ residual resistance is due to PdAu bling. The transition is gradual above 0.8 Ω, which is useful for polarization angle calibration with high power loading. The temperature change from 0.8 Ω to 0.5 Ω is about 5.1 mK, which is desirable for a CMB observation with SPT. Fig. 4 (a) shows the Noise Equivalent Power (NEP) spectrum of the TES in dark test. It approximately equals the phonon noise and a 1/f noise.

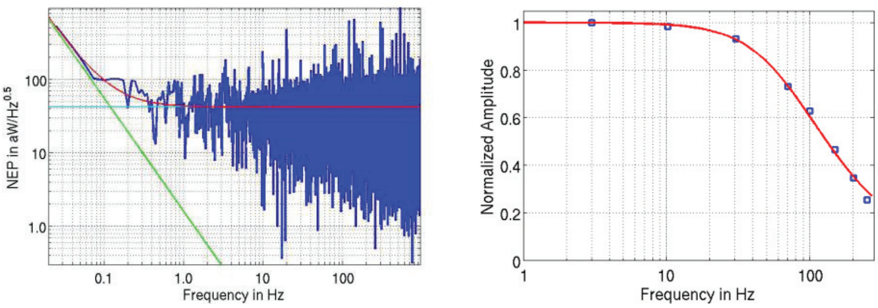

(a) (b)

Fig. 4. (a) NEP of a TES at R=0.485 Ω. The cyan is the thermodynamic phonon noise floor. The green is a 1/f noise. The red, which is the phonon noise and the 1/f noise, matches the TES noise data in blue; (b) The optical power readout efficiency with TES as a function optical power modulation frequency. The Lorentzian fit line has a time constant of 2.1 ms.

The PdAu absorber in the polarimeter dissipates electromagnetic waves polarized along it. The collected optical power and TES Joule heating power heat up the entire Si_3N_4 membrane rectangle. The temperature change caused by optical power variation is read out with the TES. The optical power readout efficiency as a function of modulated optical power frequency is measured using a chopped external thermal source for a prototype polarimeter. The normalized modulated optical power readout efficiency as a function of modulation frequency is shown in Fig. 4 (b). The TES is voltage biased at a resistance of 60% Rn. The measured 2.1 ms time constant includes thermal diffusion time from the absorber to the TES and the TES effective time constant.

The optical performance of prototype polarimeters has been tested. The polarimeters have an optical band-pass of 78–110 GHz, an optical power readout efficiency of 80%, and a cross-polarization upper limit of 1% [17].

3. Conclusion

We have designed, fabricated, and tested an absorber coupled bolometric polarimeter. The thermal conductance of the detector is understood with a boundary limited phonon transport model, its value is determined by Si_3N_4 legs dimensions, and by fraction of phonons diffusive surface reflection which is related to surface roughness [8, 14, 18]. TES transition width is tuned with Nb dots on its surface. Test data show that the absorber-coupled polarimeter has the desired performance in terms of noise, time constant, optical power readout efficiency, and cross polarization.

Acknowledgements

The authors wish to acknowledge the support from the NIST Quantum Sensors Group at Boulder for providing SQUIDs, and to thank Matthew E. Kenyon at JPL for suggestions in devices fabrication. The work at Argonne National Laboratory, including the use of facility at the Center for Nanoscale Materials (CNM), is supported by Office of Science and Office of Basic Energy Sciences of the U.S. Department of Energy, under Contract No. DE-AC02-06CH11357. The work at the University of Chicago is supported by the NSF through grant ANT-0638937 and the NSF Physics Frontier Center grant PHY-0114422 to the Kavli Institute of Cosmological Physics at the University of Chicago. It also receives generous support from the Kavli Foundation and the Gordon and Betty Moore Foundation.

References

[1] L. Richards, Journal of Applied Physics, Vol. 76, pp. 1, July 1994.
[2] J. G. Staguhn, S. H. Moseley, D. J Benford, C. A. Allen, J. A. Chervenak, T. R. Stevenson, W. T. Hsieh, Nuclear Instruments and Methods in Physics Research Section A, Vol. 520, pp. 336-339, 2004.
[3] K. D. Irwin, G. C. Hilton, D. A. Wollman, and J. M. Martinis, Journal of Applied Physics, Vol. 83, pp. 3978, April 1998.
[4] R. Crittenden, R. L. Davis, and P. J. Steinhardt, The Astrophysical Journal, Vol. 417, L13-L16, November 1993.
[5] L. Page, *et al*., The Astrophysical Journal Supplement Series, Vol. 170, pp. 335, June 2007.
[6] W. Hu and S. Dodelson, Ann. Rev. Astron. Astrophys., Vol. 40, pp. 171, 2002.
[7] R. J. Bruls, H. T. Hintzen, G. de With, and R. Metselaar, J. the European Ceramic Society, Vol. 21, pp. 263-268, 2001.
[8] G. Wang, *et al*., Advances in Cryogenic Engineering, Materials, Vol. 56, pp. 75-83, 2009.
[9] H. F. C. Hoevers, M. L. Ridder, A. Germeau, M. P. Bruijn, P. A. J. de Korte, and R. J. Wiegerink, Applied Physics Letters, Vol. 86, No. 25, 251903, June 2005.
[10] W. Holmes, J. M. Gildemeister, P. L. Richards, and V. Kotsubo, Applied Physics Letters, Vol. 72, pp. 2250-2252, May 1998.
[11] C. K. Stable, M. A. Lindeman, E. Figueroa-Feliciano, M. J. Li, N. Tralshawala, F. M. Finkbeiner, R. P. Brekosky, and J. A. Chervenak, AIP Conf. Proc., Vol. 605, pp. 223-226, 2002.
[12] K. Rostem, D. M. Glowacka, D. J. Goldie, and S. Withington, Proc. SPIE, 7020, 70200L, 2008.
[13] G. Wang, *et al*., IEEE Transaction on Applied Superconductivity, Vol. 21, pp.232, 2011.
[14] M. N. Wybourne, C. G. Eddison, and M. J. Kelly, J. Physics C: Solid State Physics, Vol. 17, pp. L607-L612, 1984.
[15] R. den Hartog, A. Golubov, D. Martin, P. Verhoeve, A. Poelaert, A. Peacock, M. Krumrey, Nuclear Instruments and Methods in Physics Research Section A, Vol. 444, pp. 28, 2000.
[16] J. E. Sadleir, S. J. Smith, S. R. Bandler, J. A. Chervenak, J. R. Clem, Physical Review Letters, Vol.104, 047003-1, 2010.
[17] A. T. Crites, *et al*., IEEE Transaction on Applied Superconductivity, Vol. 21, pp.184, 2011.
[18] C. G. Eddison and M. N. Wybourne, J. Physics C: Solid State Physics, Vol. 18, pp. 5225-5234, 1985.